Joint Interference Management and Traffic Offloading in Integrated Terrestrial and Non-Terrestrial Networks

Md Mahfuzur Rahman *Senior Member, IEEE*, Md. Zoheb Hassan *Member, IEEE*, Jeffrey H. Reed *Fellow, IEEE* , and Lingjia Liu *Senior Member, IEEE*

***Abstract*—The exponential growth of data traffic beyond the 5G era necessitates improved resource utilization for the integrated terrestrial and non-terrestrial networks (ITNTN). In this work, we consider a multi-user multiple input multiple output (MU-MIMO)-empowered 5G ITNTN network consisting of terrestrial 5G and multi-beam geostationary earth orbit (GEO) satellite-based gNBs and develop an interference management framework that allows multiple users to receive downlink data over the same resource blocks (RB) simultaneously. Our developed framework first employs a traffic offloading algorithm by leveraging the reference signal received power (RSRP) and celledge width criteria to offload traffic from terrestrial to NTN networks. Subsequently, we formulate the resultant interference management as a joint power allocation and user-RB scheduling optimization problem to maximize the network's spectral efficiency. Since the joint optimization problem is NP-hard and computationally intractable, a fractional programming-based solution is developed to obtain sub-optimal yet efficient transmit power allocation and user scheduling at terrestrial and satellite gNBs. A realistic ITNTN simulator is developed for performance evaluation by considering 3GPP channel models, antenna gains, and 5G RB numerology in rural terrestrial-GEO coexistence scenarios. Extensive simulation results confirm the efficacy of the proposed framework in managing interference and improving resource utilization at 5G ITNTN networks.**

***Index Terms*—Non-Terrestrial Network, Power allocation, Fractional Programming, Traffic Offloading.**

I. Introduction

Non-terrestrial network (NTN) collectively refers to the wireless network empowered by flying platforms, from Low Altitude Platforms (LAPs) to High Altitude Platforms (HAPs), to Low-Earth Orbit (LEO) Satellites, all the way to High-Earth Orbit (HEO) Satellites [1], [2]. NTNs can be vital in civilian and military applications by providing better navigation, communication, and remote sensing options. In the upcoming 6G networks, NTN is envisioned to have the following three use cases: (i) providing ubiquitous connectivity in rural, airborne, and maritime networks, (ii) service continuity by extending coverage of terrestrial networks, and (iii) service scalability by providing data broadcast and multi-cast services to many users [3]. Furthermore, the integration of non-terrestrial and terrestrial networks, hereafter referred to as integrated terrestrial and non-terrestrial networks (ITNTN), will be a key enabler of 5G-advanced and 6G networks with the advantages of providing omnipresent and high-quality services to both unserved and underserved regions. In particular, the ITNTN is expected to overcome the so-called "digital divide" around the globe and play a crucial role in achieving the United Nations sustainable development goals of ensuring "universal and affordable access to the Internet by 2030" [4]. The latest 3GPP TR 38.863 Release 17 [5], focuses on the co-existence aspects of NTN with the terrestrial networks (TN) within the sub-6 GHz frequencies. These guidelines, complemented by earlier releases like 3GPP TR 38.821 Release 16 [6] and 3GPP TR 38.811 Release 16 [7], have served as a driving force behind exploring NTN and TN operations simultaneously across both mmWave GHz and sub-6 GHz frequency bands.

The immense potentiality of NTN for beyond 5G networks is further evident from the increased interest of prominent industry organizations, namely, SpaceX, Amazon, OneWeb, Hughes, and Iridium, in deploying commercial NTN networks around the globe. For instance, SpaceX has achieved notable progress by deploying over 5000 LEO satellites with a vision of delivering global broadband connectivity. Their ambitious agenda involves launching an additional 12,000 LEO satellites soon, with the potential to expand to an astounding 42,000 in the future [8]. Amazon's Project Kuiper plans to launch 3236 LEO satellites to provide swift, affordable, and dependable broadband services to underserved communities worldwide [9]. In November 2023, Project Kuiper established a strategic partnership with Nippon Telegraph and Telephone Corporation (NTT DOCOMO), NTT Communications Corporation (NTT Com), and SKY Perfect JSAT Corporation (SKY Perfect JSAT). This collaboration aims to deliver advanced, dependable, and extensive satellite connectivity solutions to customers in Japan [10]. Hughes, a major player in North and South America, offers satellite services through both GEO (Geostationary Earth Orbit) and LEO constellations. Their cutting-edge Jupiter series of GEO satellites (launched in July 2023) promises an impressive boost in capacity, reaching an outstanding 500 Gbps [11].

The ITNTN networks offer a promising capability of offloading traffic from the congested TN to the NTN. Such a capability improves celledge users' performance and enables TN to provide improved data rates to its users. Several

M. M. Rahman, J. H. Reed, and L. Liu are with Wireless@Virginia Tech, Bradley Department of Electrical and Computer Engineering, Virginia Tech, VA, USA. M. Z. Hassan is with the Electrical and Computer Engineering Department, Université Laval, QC, Canada. (Corresponding author's e-mail: ljliu@vt.edu). The work of M. M. Rahman and L. Liu are supported in part by the National Science Foundation under grant CNS-2148212 and is supported in part by funds from federal agency and industry partners as specified in the Resilient & Intelligent NextG Systems (RINGS) program. This material is also based upon work supported by the National Science Foundation under NSF Award no: 2235139.

recent studies have studied the TN-to-NTN traffic offloading problem. In [12], several experiments were conducted to balance energy consumption, achievable data rates, and spectral efficiency for integrating satellites into 6G terrestrial cellular networks. In [13], LEO satellite constellations were utilized for traffic offloading and backhauling for the delay-tolerant Internet of Things (IoT) traffic. In [14], the authors explored offloading UAV traffic to the NTN, demonstrating a significant reduction in downlink outage probability for UAVs and a 12% reduction in uplink outage probability for ground users. Finally, in [15], authors introduced an innovative in-network computing paradigm using a LEO constellation-based orbital edge platform. This approach proves advantageous for both TN and NTN, especially benefiting celledge users dealing with real-time or non-real-time tasks by addressing latency challenges associated with computing tasks.

Due to the heterogeneous characteristics of TN and NTN, efficient resource management is paramount to fully capitalize the potential of ITNTN in 6G networks. For instance, in the context of space-air-ground integrated network (SAGIN), the constrained and uneven distribution of computational and communication resources impedes the capability to deliver consistent quality-of-service (QoS) assurances, especially for delay-sensitive and outage-sensitive traffic categories [16][1]. In [18], the authors investigated various issues of introducing satellite connectivity in the 5G NR system over the Ka-band. This study showed that carefully designed timing adjustments are required for the seamless execution of random access (RA) procedures, especially with a high sub-carrier spacing (SCS) and a maximum frequency offset of 66 kHz. Meanwhile, the study in [19] analyzed RA procedures for NTN NB-IoT, revealing that standard periodicity of 40 ms and 80 ms are inadequate for the expansive NTN coverage footprint and an extended periodicity of 1280 ms is required albeit with a reduced frequency of RA occasions. The co-channel interference resultant from NTN-TN spectrum sharing was also analyzed [20]. It was demonstrated via realistic simulations that a reverse pairing scenario, where NTN and TN operate in uplink and downlink over the same spectrum, respectively, reduces co-channel interference in the coexisting networks. An experimental setup was developed by employing Software-defined Radios B210 and Raspberry Pi4 to emulate a functional NTN network, providing valuable insights into the NTN system's performance and behavioral intricacies [21].

A. Motivations, Challenges, and Novelty

In the 5G era, a key motivation for integrating TN and NTN networks is to enhance celledge users' QoS. Celledge users often have poor quality of experience (QoE) due to unfavorable Radio Frequency (RF) conditions. These users experience high interference from neighboring cells, leading to a degradation in their signal quality. State-of-the-art schemes to improve the QoS of celledge users by mitigating interferences from neighboring cells often require increased overhead and time-consuming optimizations, making them challenging to implement within a constrained time frame [22]. For example, in a densely populated environment, the signal strength for celledge users oscillates rapidly between the serving cell and the surrounding cells, resulting in the so-called ping-pong effect. Strategies encompass tuning transmit power, implementing tilts, adjusting diverse offset parameters, and modifying event parameters such as a1-event, a3-event, and b1-event parameters. However, their practical implementation is confronted by the complex nature of optimizations, especially in dynamic cellular networks. The strategic traffic offloading of celledge users from TN gNBs to NTN gNBs can address this problem efficiently. Besides, in certain geographic areas, signals may be obstructed or weakened by structures like buildings, natural features such as mountains, and dense foliage like trees. In these situations, the signal strength becomes insufficient for correctly decoding the transmitted signal, causing the Reference Signal Received Power (RSRP) to drop below the threshold required for reliable signal reception. To improve the users' experience, such traffic should be redirected to the NTN.

However, interference between cross-tiers (NTN and TN components) and the same tiers (TN or NTN) present a key challenge in accommodating the ITNTN in the beyond 5G networks. The cross-tier interference can be avoided using different frequency bands for TN and NTN networks. Nevertheless, the explosive growth of user traffic is expected in the beyond 5G era, necessitating radio resources to be shared among multiple users at both TN and NTN. However, such a strategy inevitably leads to intra-cell co-channel interference and degrades users' QoS and overall capacity with reduced efficiency. Effective mitigation of such co-channel interference is of prime importance to fully exploit the potential of ITNTN for networks beyond 5G.

Motivated by this challenge, this paper's main objective is to effectively manage interference in ITNTN networks. To this end, this paper introduces the following three innovations. First, an integrated model is designed by unifying NTN and TN networks, setting the stage for a novel traffic offloading scheme. This scheme empowers celledge users with an enriched QoS by efficiently diverting their traffic from a TN to an NTN. Second, an offloading mechanism is also designed to offload traffic to NTN networks when buildings, mountains, and trees entirely or partially block the TN signals, and thus, the signal strength is too weak to decode the transmitted signal and RSRP falls below the signal-receiving threshold. Finally, a fractional programming-based algorithm is designed to optimize power allocation and resource scheduling across TN and NTN networks and mitigate intra-cell interference. Note that our previous contribution considers only NTN aspects of the problem and ignores the integration of TN and NTN [23]. In contrast, this work provides an in-depth exploration of advancements and insights of the interference management and traffic offloading solutions from TN to NTN networks.

[1]In the literature, the terminology SAGIN is used to refer to the coexistence of space network (enabled by LEO and GEO satellites), aerial network (enabled by drone, high-altitude platforms (HAPS), and balloon), and terrestrial network [17]. ITNTN, a coexistence of GEO-satellite enabled NTN and macro base station (MBS) enabled 5G cellular network, is a particular case of SAGIN.

B. Contributions and Organization

The specific contributions of this paper are summarized as follows.

1) A multi-user multiple-input multiple-output (MIMO)-empowered 5G ITNTN network compromising of terrestrial 5G and multi-beam GEO-satellite-based gNBs is considered with realistic path loss and antenna gain models. TN and NTN networks are assumed to exploit sub-6 GHz and mmWave GHz bands, respectively. In addition, we consider that both TN and NTN networks are fully loaded, and accordingly, it is required to support multiple users over the same resource blocks (RBs) to improve resource utilization efficiency. To this end, we develop a novel interference management framework by optimizing the TN-to-NTN traffic-offloading scheme and resource scheduling at both TN and NTN networks.
2) A computationally efficient algorithm is proposed to conduct offloading traffic from TN to NTN based on RSRP and celledge radius. The proposed algorithm takes the RF propagation features (such as whether it has line-of-sight (LOS) connectivity with the satellite or not) and users' positions to *dynamically* optimize the offloading decisions. Consequently, the proposed algorithm avoids aggressive traffic offloading from TN to NTN and improves resource sharing among TN users.
3) Following the offloading optimization, the intra-cell interference management problem is formulated as a joint transmit power and user-RB scheduling problem to maximize the sum capacity of both TN and NTN networks. The optimization problem is proved to be NP-hard. A novel fractional programming-based solution is developed to solve this problem sub-optimally yet efficiently. The proposed fractional programming-based solution is shown to outperform the existing fractional programming methods via simulations [24].
4) A realistic link-level ITNTN simulator considering 3GPP channel models, antenna gains, and 5G RB numerology is built to evaluate our proposed framework's performance. Extensive simulations over different traffic loading scenarios confirm the efficacy of our proposed framework in managing interference and improving the system capacity of 5G ITNTN networks.

The rest of the paper is organized as follows. A summary of the related works is provided by Section II. Section III presents a detailed system model. The proposed traffic offloading framework and intra-cell interference management problem formulation are presented in Section IV. Section V presents a detailed solution to the intra-cell interference management problem. The simulation results and concluding remarks are presented in Sections VI and VII, respectively.

II. Related Works

A. Intra-cell Interference Management

Fractional programming [24] for power allocation has shown superior performance compared to the traditional maximum power allocation strategy. When the cell transmits at its same equal maximum power for all UEs, it leads to severe multi-user interference among UEs, ultimately degrading the overall cellular performance. Fractional programming employs an efficient approach by assigning differentiated power levels for different UEs, effectively mitigating intra-cell interference and consequently elevating cellular performance. This advantage holds true, particularly in scenarios with medium to high multi-user (MU) involvement. By allocating power levels deferentially, the interference-related bottlenecks are effectively managed and the network's performance is improved. However, in the scenarios with a few UEs, the maximum power allocation strategy can be more effective due to the reduced multi-user interference among user equipments (UEs).

Considering the ongoing surge in mobile users penetration and the scarcity and costliness of the wireless spectrum, there is a need for approach to facilitate spectrum resource sharing among multiple UEs, especially in densely populated regions. Fractional programming based power allocation approach can address such a requirement as demonstrated by the state-of-the-art literature. The effectiveness of fractional programming based power allocation for mitigating intra-cell interference and improving system capacity is demonstrated for different systems including fog radio access network [25], [26], Internet-of-drones [27], [28], and IoT networks [29]. A preliminary study of this work [23] also underscores the effectiveness of fractional programming over the equal maximum power allocation strategy. Motivated by these prior studies, this work also exploits fractional programming based power allocation approach to manage intra-cell interference in dense TN and NTN networks.

B. Traffic Offloading Management - Inter-cell Interference

Optimum TN network coverage and performance provisioning is the key challenge to the service providers. Especially, TN celledge users experience extreme performance degradation due to strong interference from the neighboring TN cells. At celledge, UE moves so frequently from one cell to another, that frequent Radio Resource Control (RRC) Re-establishments cause ping-pong effects for the end users that result in key performance indicators (KPI) degradation such as increased call drops, silent calls, low mean opinion score (MOS), and more. There are several techniques to enhance KPI for celledge users such as (a) Coordinated Multi-Point Transmission (CoMP) - (1) Joint Processing (JP CoMP), (2) Coordinated Scheduling/Coordinated Beamforming (CS/CB - CoMP), or combination of these two, (b) continuous network planning and tuning for Power, Tilting, orientation, and (c) self-organizing network (SON). In Joint Processing (JP) CoMP, BSs dynamically select celledge users before transmission and jointly transmit signals to the celledge users. In CS/CB - CoMP, BSs schedule and create beams in a coordinated fashion for the end users. Time synchronization of the radio frame is the key challenge both for JP-CoMP and CS/CB-CoMP and requires a huge deal of effort and time, if not adequately synchronized, the potential benefits of CoMP cannot be fully realized [30]. As the number of cellular users grows, service providers must continually expand their network coverage and capacity. The cellular network's

capacity and coverage can be extended by building more base stations until the receiver sensitivity is achieved. While these increased base stations ensure more reliable connectivity, appropriate network design is required to avoid interference and overlapping of the signal power. This necessitates ongoing adjustments in transmit power, antenna tilting, and antenna orientation to cater to celledge users. SON enables automating the optimization of these network parameters. Nevertheless, the implementation of existing approaches (e.g., CoMP and SON) in large-scale networks is confronted by high computational complexity, signaling overhead, and cost. This paper exploits a low-complexity approach to offload celledge traffic to NTN. Such an approach can complement the existing SON and CoMP approaches by improving the QoS of delay-tolerant celledge users and reducing the congestion over TN.

C. Traffic Offloading Management - Poor Signal Strength

In both 5G and LTE networks, the evaluation of RSRP, Reference Signal Received Quality (RSRQ), and Signal-to-Interference-plus-Noise Ratio (SINR) holds paramount importance as the KPIs for critical processes like RRC Setup, RRC Re-establishment, and Handover (HO). Among these KPIs, RSRP stands out as a globally recognized metric widely employed by service providers [31], [32]. RSRP is determined at a specific point within the service area, irrespective of whether the received signal is in line-of-sight (LOS), near-line-of-sight (nLOS), or non-line-of-sight (NLOS) conditions. This measurement is crucial for assessing signal quality and ensuring optimal network performance. It helps in identifying areas with weak signal strength that may need network enhancements. Essentially, the quality of RSRP is directly proportional to the quality of LOS. In simpler terms, the better the line-of-sight conditions, the stronger the RSRP signal. However, real-world scenarios often introduce complexities where UE experiences nLOS and NLOS conditions. In these scenarios, RSRP tends to degrade, and in cases of complete NLOS, RSRP falls significantly below the threshold required for successful attach procedures. Several factors contribute to these deteriorating conditions, including the presence of high-rise buildings, mountainous terrain, and dense foliage such as trees, all of which obstruct or scatter the signal. Consequently, it becomes crucial for network operators to address these challenges to maintain reliable connectivity and optimize network performance.

In our simulation, we consider RSRP as a pivotal metric for making informed decisions regarding traffic offloading. Specifically, we consider RSRP as one of the key parameters to determine whether TN traffic should be offloaded to the NTN gNB provided NTN gNB has a direct LOS connection with ground users. By incorporating this approach, we aim to efficiently manage network resources, ensuring that TN traffic is seamlessly transferred to the NTN gNB whenever a strong LOS link is established. This strategy not only enhances network performance but also optimizes the utilization of both TN and NTN radio resources, ultimately providing a better experience for users in diverse environmental conditions.

III. System Model

A. System Overview

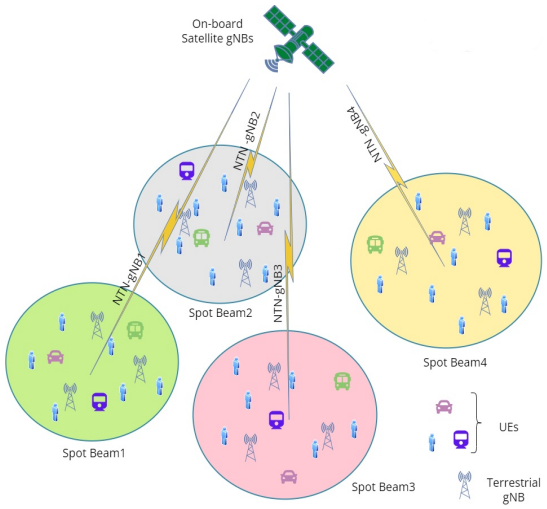

Fig. 1: Integrated NTN-TN System Architecture

TABLE I: Different interference techniques

Sl.	Network	Interference type	Mitigation Technique
1	TN	Intra-cell interference	Fractional programming
2	TN-TN	Inter-cell interference	Traffic offloading & Network Planning
3	TN-NTN	Inter-cell interference	Orthogonal operation
4	NTN-NTN	Inter-cell interference	Orthogonal operation
5	NTN	Intra-cell interference	Fractional programming

Our system considers an integrated cellular network comprising TN and NTN gNBs. In particular, we consider a geostationary satellite with the capability to operate in both single-beam (single gNB) and multi-beam modes (multiple gNBs), catering to ground UEs as depicted in Figure 1. As specified in [33] in our current analysis each spot beam provides coverage to the 19 TN omnidirectional cells, however, cell-sectoring will be considered in future work with three 120-degree sectors per TN cell/gNB. On-board satellite gNBs are orthogonal with each other with orthogonal spot beams; however, at an instance, intra-spot beam gNBs share the same resource block group (RBG). We consider different types of interference in our system such as - TN: Intra-cell interference, TN-to-TN: Inter-cell interference, TN-to-NTN: Inter-cell interference, NTN-to-NTN: Inter-cell interference, and NTN: Intra-cell interference. We mitigate all these 5 categories of interference as per Table I. Specifically, in the envisioned network scenario, UEs located within the cell-center are served by terrestrial gNBs, while those outside the cell-center are offloaded to the NTN as long as they have clear LOS links with the NTN gNB. UEs, that are outside the cell-center and do not have clear LOS links with the NTN gNB, are also served by the terrestrial gNBs. With a careful selection of terrestrial network parameters—such as frequency reuse factors, antenna downtilt angle, and celledge width—the inter-cell interference *within the cell-center* can be maintained significantly lower than the desired signal

power from the serving gNB. Thus, the TN-TN interference can be effectively mitigated by optimizing terrestrial network design parameters and offloading the celledge UEs (which are prone to interference) to the NTN. Additionally, since NTN and TN operate in entirely separate frequency bands, TN-NTN interference is eliminated. Similarly, interference among different NTN network spot beams is avoided as they use orthogonal frequency channels. Finally, intra-cell interference within TN and NTN is efficiently mitigated through the proposed fractional power allocation scheme.

To simulate a dense environment, we consider a cell radius of 1 km, i.e., the inter-cell distance is 2 km. The interconnection between UEs and the satellite is established through the robust 3GPP protocol stack, ensuring efficient and standardized communication. Simultaneously, the feeder link connecting the satellite to the gateway operates seamlessly under the satellite DVB-S2X protocol, showcasing a sophisticated and reliable communication infrastructure. The NTN gNBs operate in Frequency Range 2 (FR2) mmWave frequency band, whereas all TN gNBs operate in Frequency Range 1 (FR1) Sub-6 GHz band. The mmWave bandwidth is characterized by bw_m and sub-6 GHz bandwidth is characterized by bw_s, where $bw_m >> bw_s$. Each TN gNB supports multiple UEs that collectively share the same RBG, each RBG comprising one or multiple resource blocks (RBs). Each bandwidth, denoted as bw_m and bw_s, is associated with a specific number of RBs, represented as N_m and N_s, respectively, per the 5G numerology. The total TN sub-6 GHz RBs, N_s are grouped into M_t non-overlapping RBGs, and in each RBG, each gNB serves a group of M ground users simultaneously. The set of M_t RBG $=\{rbg_1, rbg_2, rbg_3, ..., rbg_{M_t}\}$. Each RBG consists of 1 or more numbers of RBs, then the set of each RBG with l RBs $=\{rb_1, rb_2, rb_3, ..., rb_l\}$. All NTN gNBs operate with a set of orthogonal frequencies to avoid inter-beam/inter-gNB interference. Additionally, UEs in each gNB receive differentiated power levels operating on the same RBG to mitigate intra-gNB interference. Existing literature reports that in the fading interference channel, a downlink orthogonal frequency division multiple access (OFDMA) achieves smaller sum-capacity compared to a system where multiple UE share the same frequency channel [34, Fig. 4], [35, Fig. 2]. Motivated by such a fact, we consider multiple UEs to be scheduled over the same RBG at both terrestrial and NTN gNBs, and each UE decodes its message while treating the interference from other UEs' messages as a noise. Transmit power control is applied to mitigate intra-gNB multi-user interference by allocating differentiated powers to the UEs based on their time-varying channel gains so that the sum-capacity is improved.

For our analysis, we have considered the following assumptions:

A1: Each UE at an instant can only connect to a single gNB either with TN gNB or with the NTN gNB (NTN spot beam).

A2: Each of the UEs support both FR1 and FR2 operations.

A3: The ITNTN system is designed to operate in TDD mode only, where the system parameters are updated in each iteration.

A4: For a TN gNB, at iteration t, the downlink channel gain from the k-th gNB to the l-th UE over the m_t-th RBG is modeled as $g_{k,l}^{m_t}(t) = \left|h_{k,l}^{m_t}(t)\right|^2 \gamma_{k,l,m_t}(t)$, where $h_{k,l}^{m_t}(t)$ represents small-scale complex fading due to the interference and the different multi-paths effects, and $\gamma_{k,l,m_t}(t)$ denotes large-scale fading due to the pathloss and shadowing from the k-th TN gNB to the l-th UE. However, for the NTN channel between i-th NTN spot beam and j-th UE, only long-distance pathloss and shadowing effects are considered for the downlink channel gain, i.e., $g_{i,j}^{m_n}(t) = \zeta_{i,j,m_n}(t)$.

A5: UEs only have delay-tolerant enhanced mobile broadband (eMBB) traffic, which can tolerate the high round-trip latency of the GEO satellite network.

B. TN and NTN Path Loss Models

As recommended by the 3GPP TR 38.821 [6] and 3GPP TR 38.811 [7] standards, the NTN channel is inherently different from TN channel, encompassing the integration of path losses caused by the adverse weather conditions such as rain, cloud, fog, and scintillation.

According to the 3GPP TR 38.821 standard, the path loss (in the unit of dB) for the TN link, denoted by L_t, can be expressed as

$$L_t = L_{basic} + L_{entry}, \tag{1}$$

where L_{basic} and L_{entry} are the TN basic path loss component and the building entry loss in the dB unit, respectively. The basic path loss component corresponds to the signal propagation through the surrounding clutters and shadowing, which inherently depends on the distance between the TN gNB and UE. Without a loss of generality, we consider all of our scenarios to be outdoor, and the impact of clutter loss is minimal. Therefore, we do not include the clutter path loss in calculating L_{basic}. Moreover, due to the consideration of only outdoor scenarios, L_{entry} is also disregarded. Shadow fading in the dB unit, following a zero-mean Gaussian distribution with a standard deviation of 4 dB, is considered to calculate the value of L_{basic}. The value of L_{basic} is calculated using the path loss equation mentioned within Table 7.4.1-1 of 3GPP TR 38.901 V16.1.0 - Study on channel models for frequencies from 0.5 to 100 GHz, Release 16, for Rural Macro scenarios under the LOS condition. The large-scale fading coefficient from the k-th TN gNB to the l-th UE is obtained as $\gamma_{k,l,m_t}(t) = 10^{-\frac{L_t}{10}}$.

Meanwhile, for the NTN link, the path loss (in the unit of dB), denoted by L_n, can be expressed as

$$L_n = L_{basic'} + L_{entry'} + L_{gas} + L_{scin}, \tag{2}$$

where $L_{basic'}$ is the NTN basic loss component in dB over the LOS link, $L_{entry'}$ is the NTN building entry loss in dB, L_{gas} is the gaseous loss in dB, and L_{scin} is the scintillation loss due to the radio wave propagation between different atmospheric layers in dB. As per the 3GPP TR 38.811 standard, All gaseous mediums severely affect radio wave propagation at frequencies higher than 52 GHz, and our considered band for NTN is 20 GHz, which is far below 52 GHz. As such, the gaseous effect, i.e., L_{gas}, can be ignored. Moreover, since we consider that all of our scenarios are outdoors with a clear sky, both L_{scin} and $L_{entry'}$ can be ignored. Table 6.6.2-2 of 3GPP TR 38.811

V15.4.0 shows that the Shadow fading (in the dB unit) follows a zero-mean Gaussian distribution with a standard deviation of 4 dB. As per [7, eq. 6.6-2], the expression for the LOS basic path loss component of the NTN link (in the dB unit) is determined as

$$L_{basic'} = 32.45 + 20log_{10}(d) + 20log_{10}(f_c), \quad (3)$$

where f_c is the operating frequency in GHz unit, and d is the propagation distance in the meter unit. The large-scale fading coefficient from the i-th NTN spot beam to j-th UE is obtained as $\zeta_{i,j,m_n}(t) = 10^{-\frac{L_n}{10}}$.

C. Achievable Data Rate

Each gNB in TN and NTN transmits differentiated power to its corresponding UEs. In particular, the data streams, s_n and s_t are independently encoded for N_n NTN UEs and N_t TN UEs, respectively. After linear precoding, signal s_n for N_n NTN UEs is transmitted over the same RBG by the NTN spot beam (NSB); similarly, signal s_t of the N_t TN UEs is transmitted over the same RBG by the TN gNB. Signals transmitted from both the i-th NSB and the k-th TN gNB are expressed as $x_i = \sum_{j=1}^{J} \sqrt{G_n P_{i,j,n}} s_n$ and $x_k = \sum_{l=1}^{L} \sqrt{G_t P_{k,l,t}} s_t$, respectively. Here, G_n and G_t are the uniform Gain for NTN and TN gNB antennas respectively, $P_{i,j,n}$ is the NTN gNB transmit power from i-th NSB to the j-th UE and $\mathbf{P_{i,j,n}} = [P_{i,1,n}, P_{i,2,n}, P_{i,3,n}, ..., P_{i,J,n}]$ is the power profile for all the UEs associated with the i-th NSB, whereas $P_{k,l,t}$ is the TN gNB transmit power from k-th TN gNB to the l-th UE and $\mathbf{P_{k,l,t}} = [P_{k,1,t}, P_{k,2,t}, P_{k,3,t}, ..., P_{k,L,t}]$ is the power profile for all the UEs associated with the k-th TN gNB. At iteration t, received signals at j-th and l-th UEs are expressed as

$$\begin{aligned} \mathrm{y}_{i,j} &= \sqrt{g_{i,j}^{m_n}(t)} x_{i,j} + n_0, \\ \mathrm{y}_{k,l} &= \sqrt{g_{k,l}^{m_t}(t)} x_{k,l} + n_0, \end{aligned} \quad (4)$$

where $g_{i,j}^{m_n}(t)$ is the NTN channel gain between i-th NSB and the j-th UE during m_n-th RBG whereas $g_{k,l}^{m_t}(t)$ is the TN channel gain between k-th TN gNB and the l-th UE for the duration of m_t-th RBG, n_0 is the additive white Gaussian noise with $\mathcal{N}(0, \sigma^2)$. For the sake of simplicity, all the UEs have the same noise spectral density, n_0.

Each NTN UE in the i-th NSB also receives interference from the signals transmitted for the other UEs in the same i-th NSB only. Similarly, each TN UE associated with the k-th TN gNB also receives interference from the signals of the other UEs associated with the same k-th TN gNB only; celledge UEs also receive interference from the surrounding gNB as all gNBs in a spot beam share the same RBG. However, gNBs in different spot beams are orthogonal to each other. As to neglecting NTN inter-cell interference, we consider that NSBs are non-overlapping to each other, and a UE can only connect to one gNB at a time either with NSB or with the TN gNB. As such, the rate for the NTN stream for j-th UE is expressed as

$$R_{i,j}(m_n) = \log_2 \left(1 + \frac{P_{i,j}^{m_n} g_{i,j}^{m_n}}{\sum_{\substack{j'=1 \\ j' \neq j}}^{J} \alpha_{i,j}^{m_n} P_{i,j'}^{m_n} g_{i,j}^{m_n} + \sigma^2} \right), \quad (5)$$

and rate for the TN stream for l-th UE is expressed as:

$$R_{k,l}(m_t) = \log_2 \left(1 + \frac{P_{k,l}^{m_t} g_{k,l}^{m_t}}{\sum_{\substack{l'=1 \\ l' \neq l}}^{L} \beta_{k,l}^{m_t} P_{k,l'}^{m_t} g_{k,l}^{m_t} + \sigma^2} \right), \quad (6)$$

where $\alpha_{i,j}^{m_n} \in (0,1)$ be a binary variable where $\alpha_{i,j}^{m_n} = 1$ implies that the j-th UE is scheduled to receive data from the i-th NSB over the m_n-th RBG and $\alpha_{i,j}^{m_n} = 0$ otherwise. Similarly, let $\beta_{k,l}^{m_t} \in (0,1)$ be a binary variable where $\beta_{k,l}^{m_t} = 1$ implies that the l-th UE is scheduled to receive data from the k-th TN gNB over the m_t-th RBG and $\beta_{k,l}^{m_t} = 0$ otherwise. Therefore, the total spectral sum rate is expressed as:

$$\begin{aligned} R_{total} = &\sum_{m_n=1}^{M_n} \sum_{i=1}^{I} \sum_{j=1}^{J} \alpha_{i,j}^{m_n} R_{i,j}(m_n) \\ &+ \sum_{m_t=1}^{M_t} \sum_{k=1}^{K} \sum_{l=1}^{L} \beta_{k,l}^{m_t} R_{k,l}(m_t). \end{aligned} \quad (7)$$

IV. Framework and Problem Formulation

Our developed framework sequentially performs traffic offloading and intra-cell interference management. In what follows, we first explain the mechanism of offloading traffic from TN to NTN. Afterward, the intra-cell interference management for the offloaded traffic is explained.

A. Traffic Offloading Mechanism

Note that in terrestrial networks, the celledge UEs exhibit a pronounced ping-pong effect, leading to a significant deterioration in signal quality. Furthermore, UEs exhibiting shadowing (due to blockage of the signal by large obstacles) also exhibit poor signal quality. The key idea of our proposed traffic offloading mechanism is to offload the UEs located at the celledge or experiencing heavy shadowing to the NTN. As such, the received signal quality at these UEs is improved, and the remaining UEs at the terrestrial gNBs are provided with more resources. Algorithm 1 summarizes the overall traffic offloading algorithm. Here, Φ_{LOS} and Φ_{edge} are two indicator variables. In particular, $\Phi_{LOS} = 1$ if there is a LOS link between the UE and satellite and $\Phi_{LOS} = 0$ otherwise. Likewise, $\Phi_{edge} = 1$ if the UE is located at the celledge and $\Phi_{edge} = 0$ otherwise. These two variables are determined based on UEs' positions and other context variables. An overview of Algorithm 1 is as follows. If an UE does not have LOS connection with the satellite, Algorithm 1 connects it with the nearest terrestrial gNB. Otherwise, Algorithm 1 first checks whether it is located in celledge or shadowed. In either case, Algorithm 1 connects the UE to the NTN. If none of these conditions are satisfied, then Algorithm 1 connects the UE with the nearest terrestrial gNB. Algorithm 1 provides a list of associated UEs to each terrestrial gNB and GEO NSB. Note

that the optimal performance of this algorithm depends on the suitable selection of celledge radius and RSRP threshold. Such a fact will be investigated in detail in our simulations[2].

Algorithm 1 Traffic Offloading Algorithm

Initialize: UEs' positions at each terrestrial cell and calculate RSRP for all UEs to their nearest terrestrial gNBs.
for $i \leftarrow 1 : I$ **do**
  for $j \leftarrow 1 : J$ **do**
    if $\Phi_{LOS} == 0$ **then**
      Assign the j-th UE to the i-th terrestrial gNB.
    else
      if $\Phi_{edge} == 1$ **then**
        Assign the j-th UE to the NSB.
      else
        if RSRP $<$ Threshold **then**
          Assign the j-th UE to the NSB
        else
          Assign the j-th UE to the i-th terrestrial gNB.
        end if
      end if
    end if
  end for
end for
Output: List of the associated UEs at the terrestrial gNBs and GEO NSBs.

Remark 1: In Algorithm 1, depending on the UE's position and environmental context, a UE is either connected to the NSB or the nearest terrestrial gNB. The reason for a UE being associated with the nearest terrestrial gNB is explained below. In wireless communications, the received signal strength decreases with the increasing propagation distance [36]. In our networking scenario, each terrestrial cell's signal strength is confined to its cell-center[3]. UEs located at the celledge or in the shadowed areas (i.e., where the RSRPs at the UEs fall below a specified threshold) are offloaded to the NTN network, provided they maintain LOS links with the NSB. Consequently, the cell-centered UEs (those not at the celledge or in the shadowed regions) experience the strongest signal strength from the centrally located gNB, since it is positioned at the minimum distance from these UEs. Therefore, associating these UEs to their nearest terrestrial gNBs is equivalent to associating based on signal strength. This approach simplifies the simulation since it is no longer needed to measure the signal strength from multiple gNBs. Additionally, distance-based association reduces computational complexity compared to real-time signal strength measurements.

Remark 2: The conventional approaches to improve QoS for celledge UEs, such as CoMP have certain limitations. In particular, the UEs at the edge of CoMP clusters still receive substantial inter-cluster interference. The implementation of CoMP requires the CSI for downlink precoding and data traffic to be sent from a centralized controller to the clustered APs over low-latency backhaul links. Such a fact notably increases the implementation complexity and cost of CoMP for large-scale networks. In contrast to CoMP, our proposed ITNTN approach aims to provide QoS to the celledge UEs by offloading them to the NSBs as long as there is a LOS connection between the celledge UE and satellite. Such an approach requires reduced implementation cost, signaling overhead, and computational complexity compared to CoMP. Our proposed approach also offloads shadowed UEs to the NSB by measuring RSRP and checking for LOS connection to the satellite transmitter. Therefore, our ITNTN approach can improve the QoS of both celledge and non-celledge shadowed UEs. Note that there is significant interest from policymakers, operators, and standardization bodies in enabling satellite-to-mobile connectivity in the beyond 5G and 6G networks. For example, in the US, the FCC recently approved a direct-to-smartphone regulatory framework that allows satellite operators to provide connectivity to UEs outside of cellular tower coverage [37]. Consequently, our ITNTN approach aligns with the design efforts of the next-generation cellular network.

[2]It is noteworthy that the celledge UEs or shadowed UEs, who do not have clear LOS links with the NTN gNBs, still associate with the terrestrial gNBs and these UEs may suffer inter-cell interference. However, managing inter-cell interference for such UEs is beyond the scope of the current study and it will be considered in our future work.

[3]For simplicity, we define each cell as a circular area with radius R_{cell} and a celledge width of R_{edge}. Thus, the radius of the cell-center around the terrestrial gNB is $R_{cell} - R_{edge}$.

B. Problem Formulation: Intra-cell Interference Management

For the offloaded traffic obtained from Algorithm 1, the intra-cell interference management is formulated as an optimization problem of maximizing the network's sum-capacity by jointly optimizing transmit power allocation and user-RBG scheduling at the TN gNBs and NSBs. To this end, we consider the following constraints.

(1) **Transmit power allocation constraints:** Let $P_{i,max}$ and $P_{k,max}$ be the maximum transmit power limit for the i-th NSB and the k-th TN gNB, respectively. Accordingly, we obtain the following transmit power allocation constraints:

$$\begin{aligned} &\text{(C1a)} \quad \sum_{m_n=1}^{M_n} \alpha_{i,j}^{m_n} P_{i,j}^{m_n} \leq P_{i,max}, \forall i \in \mathcal{I}, \forall j \in \mathcal{J} \\ &\text{(C1b)} \quad \sum_{m_t=1}^{M_t} \beta_{k,l}^{m_t} P_{k,l}^{m_t} \leq P_{k,max}, \forall k \in \mathcal{K}, \forall l \in \mathcal{L} \end{aligned} \tag{8}$$

(2) **RBG allocation constraints:** We obtain the following RBG allocation constraints for both terrestrial gNBs and NSBs

$$\text{(C2a)} \sum_{j=1}^{J} \alpha_{i,j}^{m_n} \geq 1, \forall m_n \in \{1, 2, \cdots, M_n\}, \forall i \in \mathcal{I}, \tag{9}$$

$$\text{(C2b)} \sum_{l=1}^{L} \beta_{k,l}^{m_t} \geq 1, \forall m_t \in \{1, 2, \cdots, M_t\}, \forall k \in \mathcal{K}, \tag{10}$$

$$\text{(C3a)} \sum_{m_n=1}^{M_n} \alpha_{i,j}^{m_n} \geq 1, \forall j \in \mathcal{J}, \forall i \in \mathcal{I}, \tag{11}$$

and

$$\text{(C3b)} \sum_{m_t=1}^{M_t} \beta_{k,l}^{m_t} \geq 1, \forall l \in \mathcal{L}, \forall k \in \mathcal{K}. \tag{12}$$

Here C2a and C2b constraints imply that the a given RBG can accommodate more than one UEs at both terrestrial gNBs and NSBs. Likewise, the constraints C3a and C3b imply that at both terrestrial gNBs and NSBs, a given UE can be scheduled

to more than one RBGs at a given time. These constraints together ensure a more generalized UE-RBG scheduling in the network compared to the conventional orthogonal (e.g., OFDMA) transmission scheme and thus, can support a high density of traffic in ITNTN networks. The system utility function is expressed as

$$f(\boldsymbol{p}, \boldsymbol{\alpha}, \boldsymbol{\beta}) = R_{total}. \tag{13}$$

In (13), $\boldsymbol{p}$, $\boldsymbol{\alpha}$, and $\boldsymbol{\beta}$ represent the vector of power allocation variables for all terrestrial gNBs and NSB, the vector of RBG scheduling variables for all terrestrial gNBs, and the vector of RBG scheduling variables for all NSBs, respectively. The resource optimization problem to maximize system utility function by jointly optimizing transmit power allocation and RBG scheduling is formulated as

$$\begin{aligned} \text{P0:} \max_{\boldsymbol{p}\geq 0, \boldsymbol{\alpha}, \boldsymbol{\beta} \in \{0,1\}} & f(\boldsymbol{p}, \boldsymbol{\alpha}, \boldsymbol{\beta}) \\ \text{s.t.} \quad & \text{(C1a), (C1b) (C2a), (C2b), (C3a), (C3b).} \end{aligned} \tag{14}$$

Theorem 1. *P0 is an NP-hard optimization problem.*

Proof: The proof is provided in Appendix A.

Since P0 is NP-hard, its global optimal solution is computationally intractable for practical systems. Accordingly, we decompose P0 into two sub-problems for transmit power allocation and RBG scheduling. A sub-optimal yet efficient solution to P0 can be obtained by alternately solving these two sub-problems. In the ensuing analysis, the solutions to the sub-problems are developed.

V. Proposed Solution

A. Sub-problem I: Transmit power allocation

Recall that interference between terrestrial gNB and NTN gNB is eliminated as these two networks operate in orthogonal frequency bands. Hence, the utility function (7) can be linearly decomposed into the following two sub-utility functions.

$$f_1(\boldsymbol{p}, \boldsymbol{\alpha}) = \sum_{m_n=1}^{M_n} \sum_{i=1}^{I} \sum_{j=1}^{J} \alpha_{i,j}^{m_n} \log_2 \left(1 + \frac{P_{i,j}^{m_n} g_{i,j}^{m_n}}{\sum_{\substack{j'=1 \\ j' \neq j}}^{J} \alpha_{i,j'}^{m_n} P_{i,j'}^{m_n} g_{i,j'}^{m_n} + \sigma^2} \right), \tag{15}$$

and

$$f_2(\boldsymbol{p}, \boldsymbol{\beta}) = \sum_{m_t=1}^{M_t} \sum_{k=1}^{K} \sum_{l=1}^{L} \beta_{k,l}^{m_t} \log_2 \left(1 + \frac{P_{k,l}^{m_t} g_{k,l}^{m_t}}{\sum_{\substack{l'=1 \\ l' \neq l}}^{L} \beta_{k,l'}^{m_t} P_{k,l'}^{m_t} g_{k,l'}^{m_t} + \sigma^2} \right). \tag{16}$$

Therefore, for the given UE-RBG scheduling, the optimization problem P0 can be decomposed into the following two independent sub-problems.

$$\text{P1:} \max_{\boldsymbol{p}\geq 0} f_1(\boldsymbol{p}, \boldsymbol{\alpha}) \text{ s.t.} \quad \text{(C1a).} \tag{17}$$

and

$$\text{P2:} \max_{\boldsymbol{p}\geq 0} f_2(\boldsymbol{p}, \boldsymbol{\beta}) \text{ s.t.} \quad \text{(C1b).} \tag{18}$$

P1 and P2 provide transmit power allocations to maximize the sum-capacity of NTN and TN networks, respectively. Both optimization problems have the same structure and therefore, they can be solved identically. However, due to the space constraint, here we present only the solution to P1 (for the NTN networks) and a solution to P2 (for the TN networks) can be obtained similarly.

We first consider the following non-linear optimization problem.

$$\begin{aligned} \text{P1.1:} \max_{\boldsymbol{p}\geq 0, \boldsymbol{x_j}\geq 0} & f_3(\boldsymbol{p}, \boldsymbol{\alpha}, \boldsymbol{x}) \\ \text{s.t.} \begin{cases} \text{(C1a)} \\ x_j = \frac{A_j(\boldsymbol{p})}{B_j(\boldsymbol{p})}), \forall j \in \{1, 2 \cdots, J\}. \end{cases} \end{aligned} \tag{19}$$

where $\boldsymbol{x}$ is an auxiliary variable and $f_3(\cdot)$ is defined as

$$\begin{aligned} f_3(\boldsymbol{p}, \boldsymbol{\alpha}, \boldsymbol{x}) = & \sum_{i=1}^{I} \sum_{j=1}^{J} \alpha_{i,j}^{m_n} \log_2 (1 + x_j) \\ & - \sum_{i=1}^{I} \sum_{j=1}^{J} \alpha_{i,j}^{m_n} x_j + \sum_{i=1}^{I} \sum_{j=1}^{J} \frac{\alpha_{i,j}^{m_n} (x_j - 1) A_j}{A_j - B_j}, \end{aligned} \tag{20}$$

where $A_j = P_{i,j}^{m_n} g_{i,j}^{m_n}, B_j = \sum_{\substack{j'=1 \\ j' \neq j}}^{J} \alpha_{i,j'}^{m_n} P_{i,j'}^{m_n} g_{i,j'}^{m_n} + \sigma^2$. Note that for any feasible transmit power, $\boldsymbol{p}$, we obtain $f_3(\boldsymbol{p}, \boldsymbol{x}, \boldsymbol{\alpha}) = f_1(\boldsymbol{p}, \boldsymbol{\alpha})$ as long as $x_j = \frac{A_j(\boldsymbol{p})}{B_j(\boldsymbol{p})}, \forall j$ is satisfied. Using such an observation, we introduce the following theorem.

Theorem 2. *The problems P1 and P1.1 have the same optimal solution.*

Proof: The proof is provided in Appendix B.

Leveraging *Theorem 2*, for the given user-RBG scheduling, we can obtain transmit power allocation by solving P1.1 instead of P1. The key reason we are interested in solving P1.1 is that it maximizes a *sum-of-ratios* instead of *sum-of-functions-of-ratios*. Note that although maximizing a *sum-of-ratios* is NP-complete, such a problem can be efficiently solved by applying the quadratic transformation of fractions. After applying to quadratic transformation of fractions [24, Corollary 1], an equivalent optimization problem to P1.1 is obtained as

$$\begin{aligned} \text{P1.2:} \max_{\boldsymbol{p}\geq 0, \boldsymbol{x_j}\geq 0} & f_4(\boldsymbol{p}, \boldsymbol{\alpha}, \boldsymbol{x}, \boldsymbol{y}) \\ \text{s.t.} \begin{cases} \text{(C1a)} \\ x_j = \frac{A_j(\boldsymbol{p})}{B_j(\boldsymbol{p})}), \forall j \in \{1, 2 \cdots, J\}. \end{cases} \end{aligned} \tag{21}$$

where $\boldsymbol{y}$ is an auxiliary variable and $f_4(\boldsymbol{p}, \boldsymbol{\alpha}, \boldsymbol{x}, \boldsymbol{y})$ is obtained as

$$\begin{aligned} f_4(\boldsymbol{p}, \boldsymbol{\alpha}, \boldsymbol{x}, \boldsymbol{y}) = & \sum_{i=1}^{I} \sum_{j=1}^{J} (\alpha_{i,j}^{m_n} \log_2 (1 + x_j) \\ & - \alpha_{i,j}^{m_n} x_j + 2 y_j \sqrt{\alpha_{i,j}^{m_n} (x_j - 1) A_j} - y_j^2 (A_j - B_j)), \end{aligned} \tag{22}$$

P1.2 can be solved by alternately updating the variables $\boldsymbol{y}$, $\boldsymbol{x}$, and $\boldsymbol{p}$. The detailed solutions are summarized as follows.

Optimal $\boldsymbol{y}$: For the given $\boldsymbol{x}$ and $\boldsymbol{p}$, P1.1 is a convex optimization problem with respect to $\boldsymbol{y}$. Therefore, by directly

applying the Karush-Khun-Tucker (KKT) conditions, the optimal $\boldsymbol{y}$ is obtained as

$$y_j^* = \sqrt{\frac{\alpha_{i,j}^{m_n} x_j}{P_{i,j}^{m_n} g_{i,j}^{m_n} - (\sum_{\substack{j'=1 \\ j' \neq j}}^{J} \alpha_{i,j'}^{m_n} P_{i,j'}^{m_n} g_{i,j'}^{m_n} + \sigma^2)}}, \forall j. \quad (23)$$

Optimal $\boldsymbol{x}$: Since the optimal solution to P1.1 must satisfy all the constraints, the optimal value of $\boldsymbol{x}$ is obtained as

$$x_j^* = \frac{P_{i,j}^{m_n} g_{i,j}^{m_n}}{\sum_{\substack{j'=1 \\ j' \neq j}}^{J} \alpha_{i,j'}^{m_n} P_{i,j'}^{m_n} g_{i,j'}^{m_n} + \sigma^2}, \forall j. \quad (24)$$

Optimal $\boldsymbol{p}$: For the given $\boldsymbol{y}$ and $\boldsymbol{x}$, P1.1 is a convex optimization problem with respect to $\boldsymbol{p}$. Therefore, by setting $\frac{\partial f_4}{\partial p} = 0$, we obtain

$$P_{i,j}^{m_n{}^*} = \frac{g_{i,j} \alpha_{i,j}^{m_n} (x_j - 1)}{y_n^2 (g_{i,j} - \sum_{\substack{j'=1 \\ j' \neq j}}^{J} \alpha_{i,j'}^{m_n} g_{i,j'})}. \quad (25)$$

Note that the aforementioned power allocation may not satisfy the transmit power allocation constraint (C1a). Hence, the refined transmit power allocations are obtained as

$$P_{i,j}^{m_n{}^*} = \frac{P_{i,j}^{m_n{}^*}}{\sum_{j=1}^{J} P_{i,j}^{m_n{}^*}} P_{i,max}, \forall j \in \mathcal{J}, \forall i \in \mathcal{I}. \quad (26)$$

A stationary point to P1 can be obtained by iteratively updating $\boldsymbol{y}$, $\boldsymbol{x}$, and $\boldsymbol{p}$ using (23), (24), and (26), respectively. However, such a stationary point is a sub-optimal solution to P1.

B. Sub-problem II: UE-RBG scheduling

For the given transmit power allocation, the optimal UE-RBG scheduling for NTN networks is obtained as

$$\text{P2: } \max_{\boldsymbol{\alpha} \in \{0,1\}} f_1(\boldsymbol{p}, \boldsymbol{\alpha}) \text{ s.t. } \quad \text{(C2a), (C3a).} \quad (27)$$

Considering $\boldsymbol{y}$ and $\boldsymbol{x}$ are obtained from (23) and (24), respectively, we can write $f_1(\boldsymbol{p}, \boldsymbol{\alpha}) = f_4(\boldsymbol{p}, \boldsymbol{\alpha}, \boldsymbol{x}, \boldsymbol{y})$. Consequently, the optimal solution to (27) is obtained as

$$\alpha_{i,j}^{m_n} = \begin{cases} 1, & \text{if } f_4(\boldsymbol{p}, \{\boldsymbol{\alpha}_{(-)}, \alpha_{i,j}^{m_n}\}\boldsymbol{x}, \boldsymbol{y})|_{\alpha_{i,j}^{m_n}=1} \\ & > f_4(\boldsymbol{p}, \{\boldsymbol{\alpha}_{(-)}, \alpha_{i,j}^{m_n}\}\boldsymbol{x}, \boldsymbol{y})|_{\alpha_{i,j}^{m_n}=0} \\ 0, & \text{otherwise} \end{cases} \quad (28)$$

where $\boldsymbol{\alpha}_{(-)}$ indicates the set of all UE-RBG scheduling variables except $\alpha_{i,j}^{m_n}$. By simplifying (28), the optimal UE-RBG scheduling between the j-the UE and the m_n-th RBG at the i-th NTN gNB, $\forall j, m_n, i$, is obtained as

$$\alpha_{i,j}^{m_n} = \begin{cases} 1, \text{ if } \Delta_{i,j}^{m_n} > 0; \\ 0, \text{ Otherwise} \end{cases} \quad (29)$$

where $\Delta_{i,j}^{m_n} = \log_2(1 + x_j^*) - x_j^* + 2y_j^* \sqrt{(x_j^* - 1) A_j(\boldsymbol{p}^*)} - (y_j^*)^2 (A_j(\boldsymbol{p}^*) - B_j(\boldsymbol{p}^*))$.

Based on the aforementioned solutions, the overall algorithm to obtain the transmit power allocation and UE-RBG scheduling for the NTN networks is summarized as Algorithm 2. The computational complexity of Algorithm 2 is primarily influenced by the execution of the for loop. At each iteration, the for loop is executed a total of I times. During each execution, Steps 1, 2, and 3 require J, J, and $M_n J$ computations, respectively. Consequently, the overall computational complexity of Algorithm 2 is $\mathcal{O}(I(J + J + M_n J)) = \mathcal{O}(IJM_n)$. A similar algorithm is also developed to obtain the transmit power allocation and UE-RBG scheduling for maximizing sum-rate within the TN networks. Due to the space limitation, such an algorithm is omitted.

Algorithm 2 Transmit power allocations and UE-RBG scheduling for NTN networks

Input: Obtain the CSI $\{g_{i,j}^{m_n}\}$, $\forall j \in \{1, 2 \cdots, J\}, \forall m_n \in \{1, 2, \cdots, M_n\}, \forall i \in \{1, 2, \cdots, I\}$. Set the maximum number of iterations T_{max} and tolerance limit δ.
Step 0: Initialize $P_{i,j}^{m_n}$ and x_j to feasible values, $\forall j, m_n, i$; iteration index $t = 1$.
for $i \in 1 : I$ **do**
  repeat
    Step 1: Update $y_j, \forall j \in \{1, 2 \cdots, J\}$ by (23).
    Step 2: Update $x_j, \forall j \in \{1, 2 \cdots, J\}$ by (24).
    Step 3: Update $P_{i,j}^{m_n}$ and $\alpha_{i,j}^{m_n}$, $\forall j \in \{1, 2 \cdots, J\}, \forall m_n \in \{1, 2, \cdots, M_n\}$ jointly by (26) and (29), respectively. Increase the iteration index $t = t + 1$.
  until $t > T_{max}$ or $|f_4^{(t+1)}(\cdot) - f_4^{(t)}(\cdot)| \leq \delta$.
  end for
  Output: $P_{i,j}^{m_n}$ and $\alpha_{i,j}^{m_n}$, $\forall j \in \{1, 2 \cdots, J\}, \forall m_n \in \{1, 2, \cdots, M_n\}, \forall i \in \{1, 2, \cdots, I\}$.

Theorem 3. *Algorithm 2 obtains a converged solution to the optimization problem P0.*

Proof: The proof is provided in Appendix C.

VI. Performance Evaluation

A. Simulation Setup

We develop a comprehensive cellular system that seamlessly integrates TN and NTN Base Stations (BSs). Our system exhibits compatibility with various Radio Access Technologies (RATs), including 4G (LTE), 5G (NR), and others. Despite this versatility, our analysis is specifically focused on the 5G system. In our configuration, we design the satellite onboard NTN gNB to function as a regenerative payload, while remote NTN gNB can be adapted to serve as a transparent payload with certain modifications. The RMa TN gNBs are set at a fixed height of 35m. UEs are evenly distributed around the gNB, both horizontally and vertically, with a maximum height of 1.5m and a radial displacement from the gNB capped at 1 km. Each UE is a single antenna system whereas each gNB is a massive MIMO antenna system. The elevation angle for each UE is calculated based on its random position with the satellite.

Following the specifications outlined in 3GPP TR 38.901 [33], TN gNBs usually transmit at 46 dBm at 2 GHz, while NTN gNBs usually transmit at 10 dBm at 20 GHz. However, for the sake of performance comparison between the ITNTN system and the TN system, we consider both gNB types transmitting at 46 dBm. The antenna gain for both TN and NTN antennas is set at 20 dBi. Unlike LTE, 5G introduces various numerologies with distinct specifications, as detailed

TABLE II: Supported transmission numerologies as per 3GPP TS 38.211 Release 17 [40].

μ	$\Delta f = 2^{\mu}.15$ [kHz]	Cyclic Prefix
0	15	Normal
1	30	Normal
2	60	Normal, Extended
3	120	Normal
4	240	Normal
5	480	Normal
6	960	Normal

TABLE III: Simulation parameters.

Sl.	Features	Values
1	MU-MIMO	2,5,8
2	No of Satellite	1
3	Satellite type	GEO
4	Satellite altitude	35786 km
5	No of Beams	1 and 4
6	gNB per beam	19
7	Elevation angles	varies
8	Beam radius, NTN	10 km
9	Cell radius, TN	2 km
10	Height, TN gNB	35 m
11	Height, UE	1.5 m
12	Max Power, TN gNB	46 dBm
13	Max Power, NTN gNB	46 dBm, 10 dBm
14	Ant gain	20 dBi
15	Frequency, TN	2 GHz
16	Frequency, NTN	20 GHz
17	Bandwidth	100 MHz
18	Sub-carrier Spacing, SCS	60 kHz
19	No of PRB	132
20	No of iterations	20
21	Cut-off RSRP	-85 dBm to -105 dBm
22	Hysteresis	-5 dBm
23	Celledge width	100 m to 600 m

in Table II. For our simulations, we adopt a sub-carrier spacing (SCS) of 60 kHz and a 100 MHz bandwidth for both FR1 operations in TN and FR2 operations in NTN. As per 3GPP TS 38.101-1 [38] and 3GPP TS 38.101-2 [39], the maximum transmission bandwidth configuration (number of resource blocks, NRB) in FR1 with 60 kHz SCS is 135, and in FR2, it is 132. However, for simplicity, we consider the maximum transmission bandwidth (NRB) to be the same for both FR1 and FR2 with 60 kHz SCS and set at 132 NRB. Tables IV and V list the maximum transmission bandwidth (NRB) for the FR1 and FR2 bands respectively.

For a comprehensive overview, all simulation parameters are summarized in Table III.

B. Resource Management

1) Intra-cell Interference Management: Fractional programming power allocation demonstrates superior performance compared to maximum power allocation, which equally allocates the maximum available power among all the UEs regardless of their channel conditions. Transmitting with the maximum power for all the UEs within a cell can lead to severe intra-cell interference issues, consequently diminishing cellular performance. In contrast, our proposed fractional programming technique (i.e., Algorithm 2) strategically allocates differentiated power levels to UEs based on UEs' channel gains. Such an approach can effectively mitigate interference and enhance overall cellular performance. This phenomenon holds true, particularly in medium to high physical resource block (PRB) utilization scenarios. In scenarios with a lower number of PRB utilization, equal maximum power allocation proves to be more effective due to reduced interference between UEs. For all the presented simulation results, the high, medium, and low PRB utilization refers to the scenarios where 8, 5, and 2 UEs are simultaneously scheduled over a PRB, respectively. Consistent to the aforementioned statements, Fig. 2 shows that our proposed fractional programming approach converges and outperforms both the conventional fractional programming approach and the maximum power allocation approach in high and medium PRB utilization scenarios.

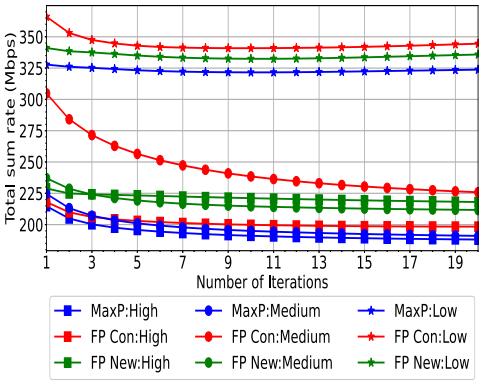

Fig. 2: Sum rate comparison between FP new algorithm with benchmark algorithms in TN system (celledge width: 200m).

2) Traffic Offloading - Comparison between ITNTN and TN: Recall, we employ a traffic offloading technique that directs the celledge traffic to the NTN gNB using Algorithm 1. To access the effectiveness of such offloading mechanism, we consider celledge widths of 500 m and 200 m with a cell radius of 1 km. As shown in Fig. 3, results from these simulations reveal subtle variations in the performance graphs between the two celledge widths. For each of these celledge widths, we carefully investigate system capacity across different levels of PRB utilization, including high, medium, and low utilization scenarios. Fig. 3 shows that in high, medium, and low utilization scenarios and for different power allocation approaches, the ITNTN system achieves remarkably higher system capacity than the TN system. For example, when the celledge width is $200m$ and the proposed fractional programming approach is utilized for power allocation, the ITNTN system achieves almost 100 Mbps higher system capacity than the TN system. Such a fact is expected since ITNTN system exploits NTN radio resources to support the celledge or shadowed UEs and thereby, also reduces congestion in the TN networks. Consequently, our proposed low-complexity traffic offloading mechanism is effective in improving the system capacity.

3) Traffic Offloading - Impact of RSRP Cutoff Values: Fig. 4 illustrates the variation of spectral efficiency using various RSRP cutoff values, specifically -85 dBm, -95 dBm, and -105 dBm, with a hysteresis threshold of -5 dBm while considering high PRB utilization scenario. Fig. 5 illustrates the variation of average rate per RBG for the same RSRP cutoff values and hysteresis threshold while considering high

TABLE IV: FR1: Maximum transmission bandwidth, N_{RB} as per Release 18 [38].

SCS kHz	5 MHz	10 MHz	15 MHz	20 MHz	25 MHz	30 MHz	35 MHz	40 MHz	45 MHz	50 MHz	60 MHz	70 MHz	80 MHz	90 MHz	100 MHz
15	25	52	79	106	133	160	188	216	242	270	N/A	N/A	N/A	N/A	N/A
30	11	24	38	51	65	78	92	106	119	133	162	189	217	245	273
60	N/A	11	18	24	31	38	44	51	58	65	79	93	107	121	135

TABLE V: FR2: Maximum transmission bandwidth, N_{RB} as per 3GPP Release 18 [39].

SCS kHz	50 MHz	100 MHz	200 MHz	400 MHz	800 MHz	1600 MHz	2000 MHz
60	66	132	264	N/A	N/A	N/A	N/A
120	32	66	132	264	N/A	N/A	N/A
480	N/A	N/A	N/A	66	124	248	N/A
960	N/A	N/A	N/A	33	62	124	148

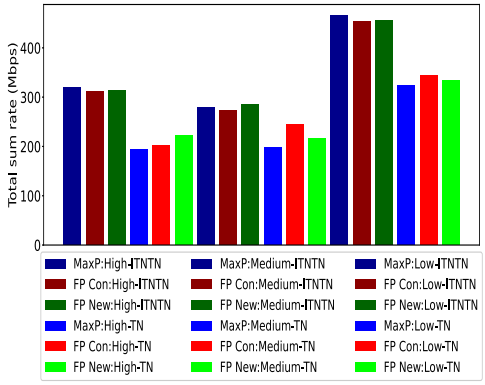

(a) Celledge width 200 m

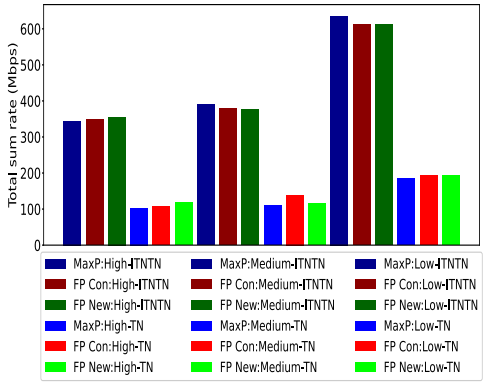

(b) Celledge width 500 m

Fig. 3: Total sum rate comparison between ITNTN and TN systems.

PRB utilization scenario. In both figures, two different celledge widths (200m and 500m) are considered. As we see in Algorithm 1, the RSRP cutoff values play a pivotal role in determining when the TN gNB would offload its traffic to the satellite onboard NTN gNB. Meanwhile, traffic offloading to the NTN gNB occurs only when a direct LOS connection with ground UEs is available. Note that as the number of UEs offloaded to NTN depends on both RSRP cutoff threshold and celledge width, different values of these parameters result in different number of UEs associated with the TN cells. Fig. 4 and Fig. 5 consistently demonstrate that convergence of our proposed fractional programming approach is guaranteed for any RSRP cutoff threshold and celledge width. This means that our proposed Algorithm 2's convergence is guaranteed for any number of UEs, i.e., Algorithm 2 is scalable.

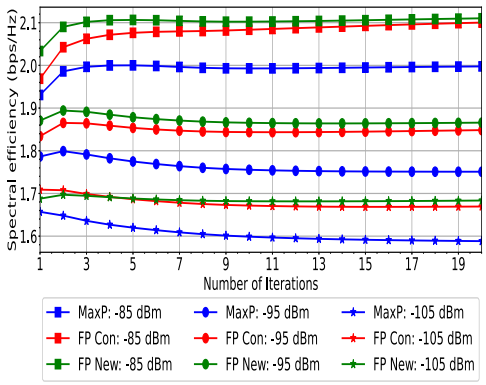

(a) Celledge width 200 m

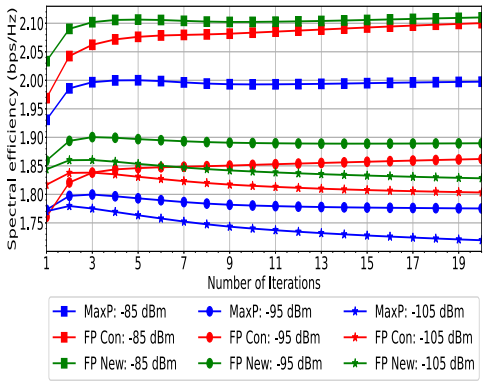

(b) Celledge width 500 m

Fig. 4: Overall spectral efficiency rate at different RSRP cutoff values (High MU MIMO).

C. Capacity Analysis

In this section, we provide simulation results on various capacity metrics for high, medium, and low PRB utilization scenarios.

1) Spectral Efficiency: Fig. 6 illustrates the spectral efficiency, expressed in bits per second per Hertz, for -95 dBm cutoff RSRP, -5 dBm hysteresis margin, and 200m celledge width. Different PRB utilization scenarios are considered. The significance of spectral efficiency becomes evident in the context of utilizing two distinct systems—one operating within the

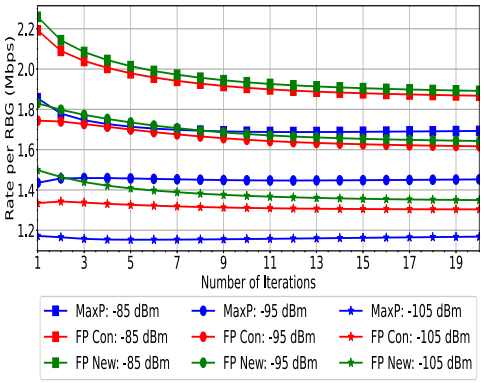

(a) Celledge width 200 m

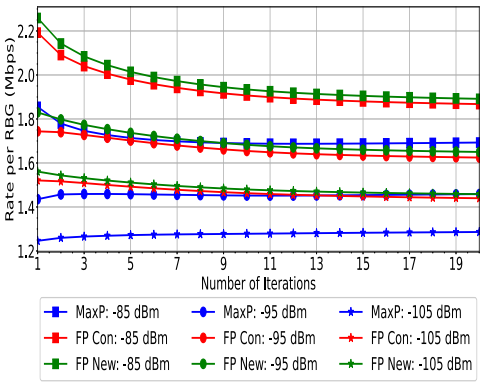

(b) Celledge width 500 m

Fig. 5: Average rate per RBG at different RSRP cutoff values (Medium MU MIMO).

sub-6 GHz frequency band and the other in the mmWave GHz frequency band. In this scenario, the utilization of spectral efficiency outweighs relying on user-perceived throughput, providing a more nuanced understanding of system performance. This approach allows for a granular assessment of data transmission efficiency, particularly crucial when dealing with diverse frequency bands. As expected, Fig. 6 shows that our proposed fractional programming-based approach also achieves higher spectral efficiency than the baseline fractional programming and maximum power allocation approaches in high and medium PRB utilization scenarios.

2) Average rate per RBG: Fig. 7 illustrates the average rate per RBG metric for -105 dBm cutoff RSRP, -5 dBm hysteresis margin, and 500m celledge width. Here, each RBG comprises only a single RB. However, our proposed framework is also applicable to scenarios where each RBG incorporates multiple RBs within the time-frequency resource grid. Fig. 7 considers three distinct scenarios, each representing different level of usage of PRBs. Similar to Fig. 6, Fig. 7 shows that our proposed fractional programming-based approach also achieves higher spectral efficiency than the baseline fractional programming and maximum power allocation approaches in high and medium PRB utilization scenarios.

3) Total sum rate of the integrated network: Fig. 8 shows the total sum rate for the ITNTN network considering -105 dBm cutoff RSRP, -5 dBm hysteresis margin, and 500m celledge width. Fig. 9 shows the total sum rate for the ITNTN network considering -95 dBm cutoff RSRP, -5 dBm

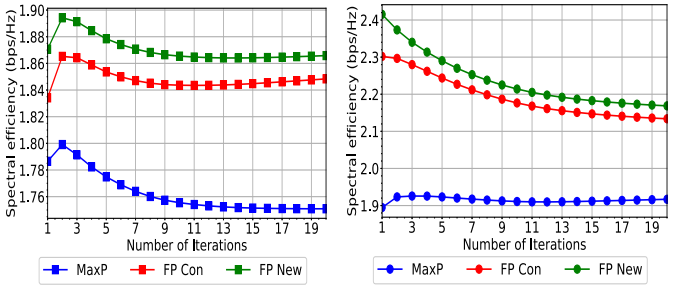

(a) High MU-MIMO (b) Medium MU-MIMO

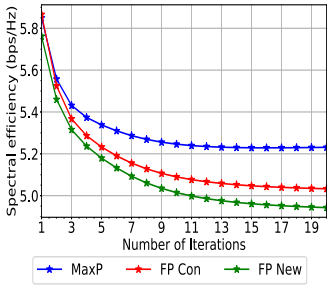

(c) Low MU-MIMO

Fig. 6: Spectral efficiency with cutoff RSRP and hysteresis of -95dBm and -5dBm respectively (celledge width 200m).

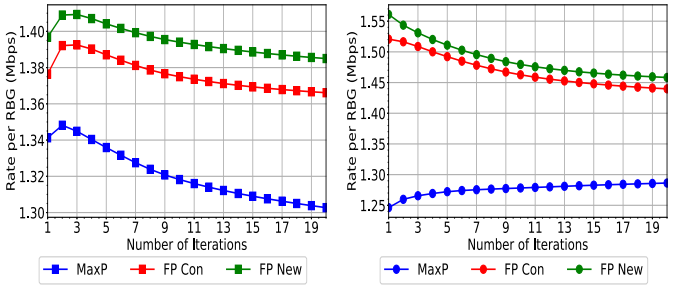

(a) High MU-MIMO (b) Medium MU-MIMO

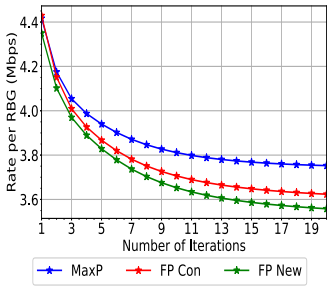

(c) Low MU-MIMO

Fig. 7: Average rate per RBG for celledge width 500 m (RSRP -105dBm, hysteresis -5dBm).

hysteresis margin, and 200m celledge width. For both figures, 100 MHz bandwidth is utilized to compute the total sum rate. Both figures show that our proposed fractional programming based approach achieves higher total system capacity than the baseline fractional programming and maximum power allocation approaches in high and medium PRB utilization scenarios. However, it is noteworthy that a complex interplay among various factors, such as bandwidth allocation, PRB

utilization, MU-MIMO configurations, celledge widths, and cutoff RSRP threshold, influences the integrated network's overall capacity. In practice, the optimal resource scheduling scheme for maximizing integrated network's sum-rate needs to be selected by taking all these factors into consideration.

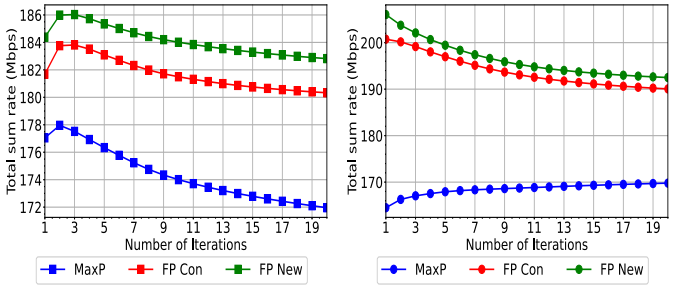

(a) High MU-MIMO (b) Medium MU-MIMO

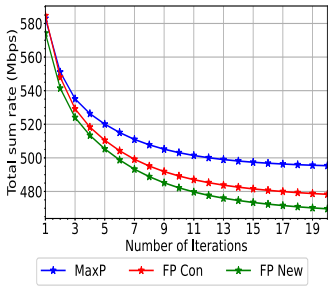

(c) Low MU-MIMO

Fig. 8: Total sum rate with cutoff RSRP and hysteresis of -105 dBm and -5 dBm, respectively (celledge width 500 m).

Fig. 10 illustrates the converged values of the total system capacity with celledge width variations from 100m to 600m while considering the high, medium, and low PRB utilization scenarios. Note that our proposed scheme offloads the celledge UEs to NTN as long as they have the clear LOS links. As a result, with the increase of celledge widths, less number of UEs are associated with the TN gNBs and most of these UEs are close to cell-centric. Due to the fact that the TN links have an order less path loss than the NTN links, the system capacity is increased with the increase of celledge width. We also observe that in low PRB utilization scenarios, our proposed power allocation algorithm is outperformed by both the MaxP and conventional FP approaches. This is due to the low likelihood of sharing PRBs among UEs, which significantly reduces intra-cell interference. The MaxP approach achieves optimal system capacity in the absence of intra-cell interference, while the conventional FP approach also performs well in scenarios with minimal PRB utilization. However, our algorithm excels in high and medium PRB utilization scenarios due to its capability to manage intra-cell interference efficiently with effective power allocation. For example, Fig. 10-b shows that for a 400m cell edge width and medium PRB utilization scenario, our proposed FP, conventional FP, and MaxP approaches achieve system capacities of 217 Mbps, 214 Mbps, and 192 Mbps, respectively. This analysis highlights our algorithm's suitability for scenarios with dense PRB usage.

In Fig. 11, we plot the variation in the converged system

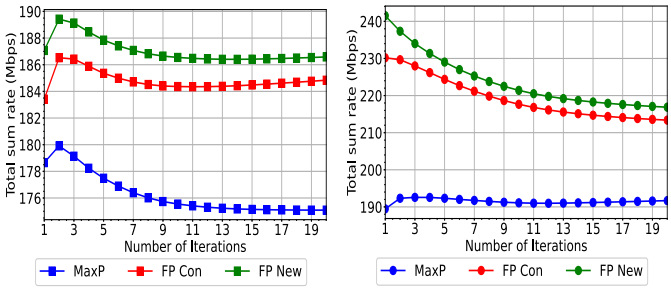

(a) High MU-MIMO (b) Medium MU-MIMO

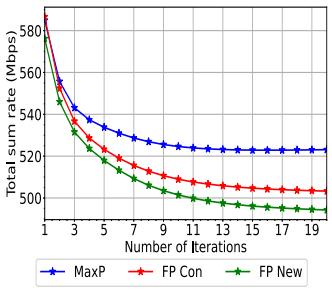

(c) Low MU-MIMO

Fig. 9: Total sum rate with cutoff RSRP and hysteresis of -95 dBm and -5 dBm, respectively (celledge width 200 m).

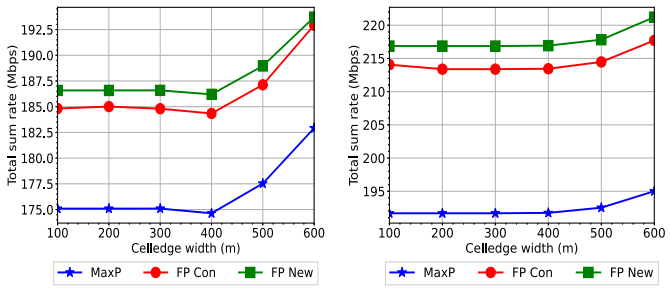

(a) High MU-MIMO (b) Medium MU-MIMO

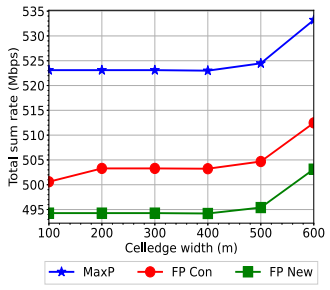

(c) Low MU-MIMO

Fig. 10: Converged total sum rate versus (vs.) celledge widths for -95dBm RSRP and -5 dBm hysteresis.

capacity of both the proposed and benchmark power allocation schemes as the cutoff RSRP varies from -85 dBm to -105 dBm across high, medium, and low PRB utilization scenarios. Again, as the cutoff RSRP is increased, the UEs that are far from TN gNB have an increased likelihood of being offloaded to the NTN. This, in turn, reduces the congestion and intra-cell interference in the TN network and improves the overall system capacity. Likewise the previous results, our algorithm demonstrates improved performance in high and medium PRB utilization scenarios by effectively managing resource blocks and mitigating interference. However, in low intra-cell interference scenarios with low PRB utilization, our algorithm shows certain capacity degradation compared to the benchmark schemes. Both Figs. 10 and 11 reveal a consistent trend: our algorithm outperforms the benchmark schemes across the entire RSRP range as PRB utilization increases. This confirms the capability of our proposed algorithm to manage resource blocks effectively and mitigate interference in dense settings where extreme PRB reuse is essential.

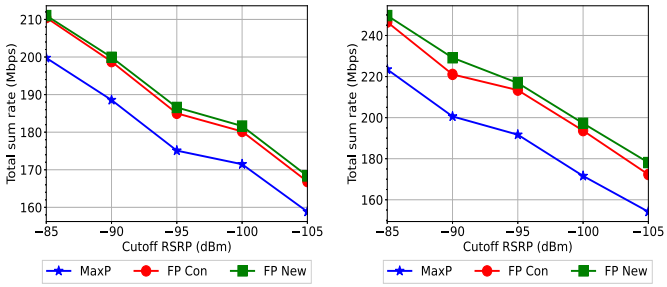

(a) High MU-MIMO (b) Medium MU-MIMO

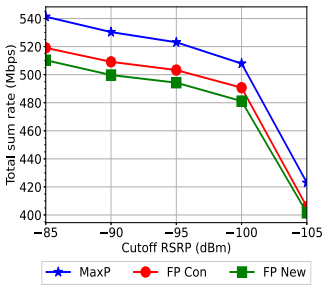

(c) Low MU-MIMO

Fig. 11: Converged total sum rate vs. cutoff RSRPs variation for 200m celledge width.)

VII. Conclusion

This paper developed an interference management framework to maximize the users' achievable throughput in the ITNTN networks with coexisting multi-antenna 5G terrestrial and multi-beam GEO satellite-mounted gNBs. We considered sub-6 GHz (FR1 band) and mmWave (FR2 band) for the operations of TN and NTN networks, respectively. Our developed framework sequentially conducts traffic offloading and intra-cell interference management. We developed an algorithm for offloading the celledge or shadowed UEs from TN gNBs to NTN by taking RSRP, celledge width, and RF propagation contexts. For the intra-cell interference management, we developed a fractional programming algorithm for conducting joint transmit power allocation and UE-RBG scheduling. Our proposed framework (a) enhances celledge and shadowed UEs' performance while efficiently using TN network's radio resources for the non-celledge UE' performance and (b) enhances the efficiency of utilization of RBGs by allowing multiple UEs to be simultaneously supported over the same RBG. We also developed a 3GPP-compliant ITNTN simulator to assess the performance of our developed interference management framework. Extensive simulation results confirmed that our interference management framework achieves better spectral efficiency, average RBG rate, and overall throughput than the benchmark schemes over the high and medium PRB utilization scenarios.

Appendix A

We assume that P0 is not an NP-hard problem and accordingly, P0 and any of its special instances must be solvable in polynomial time. We assume an efficient algorithm exists to find the UE-RBG scheduling at terrestrial gNBs and NSBs. For example, the UE-RBG scheduling can be obtained using a channel gain-based bipartite matching algorithm. Hence, P0 is reduced to a set of $|\mathcal{K}+\mathcal{I}|$ number of independent optimization problems, each for one gNB. The optimization problem for the k-th gNB is expressed as

P0.1:

$$\max_{\boldsymbol{p}\geq 0} \sum_{m=1}^{M_n}\sum_{j=1}^{J} \alpha_{i,j}^{m_n} \log_2\left(1+\frac{P_{i,j}^{m_n} g_{i,j}^{m_n}}{\sum_{\substack{j'=1\\ j'\neq j}}^{J} \alpha_{i,j}^{m_n} P_{i,j'}^{m_n} g_{k,j'}^{m_n}+\sigma^2}\right)$$
$$\text{s.t.} \sum_{m_n\in\mathcal{M}_n}\sum_{j=1}^{J} \alpha_{i,j}^{m_n} P_{i,j}^{m_n} \leq P_{i,max}, \forall m_n \in \mathcal{M}_n. \tag{30}$$

P0.1 is essentially a sum-rate maximization problem over the interference channels, which is a strong NP-hard optimization problem [41, Th. 2]. Accordingly, we obtain a stark contradiction with the initial assumption that P0 and its all variants are optimally solvable using a polynomial time algorithm. Hence, our initial assumption does not hold true, i.e, P0 must be an NP-hard optimization problem. □

Appendix B

Let $\boldsymbol{p}^*$ and $\boldsymbol{q}^*$ are the optimal solutions to the problems P1 and P1.1, respectively. We obtain the following inequality.

$$\begin{aligned} & f_3(\boldsymbol{q}^*,\boldsymbol{\alpha},\boldsymbol{x})\big|_{x_j=\frac{A_j(\boldsymbol{q}^*)}{B_j(\boldsymbol{q}^*)},\forall j} \\ &=^{(1)} f_1(\boldsymbol{q}^*,\boldsymbol{\alpha}) \leq^{(2)} f_1(\boldsymbol{p}^*,\boldsymbol{\alpha}). \end{aligned} \tag{31}$$

Here, the equality (1) is obtained based on the aforementioned observation about the equality between $f_1(\cdots)$ and $f_3(\cdot)$ functions. Note that since $\boldsymbol{q}^*$ is an optimal solution to P1.1, it will satisfy the transmit power budget constraints. As a result, $\boldsymbol{q}^*$ is a feasible solution to P1. Since $\boldsymbol{p}^*$ is an optimal solution P1, the objective function value of P1 with $\boldsymbol{p}^*$ must be larger than the the objective function value of P1 with $\boldsymbol{q}^*$. Thus, the inequality (2) must hold true.

Similarly, we can justify that the following inequality holds true as well.

$$\begin{aligned} f_1(\boldsymbol{p}^*, \boldsymbol{\alpha}) &=^{(3)} f_3(\boldsymbol{p}^*, \boldsymbol{\alpha}, \boldsymbol{x})\big|_{x_j=\frac{A_j(\boldsymbol{p}^*)}{B_j(\boldsymbol{p}^*)},\forall j} \\ &\leq^{(4)} f_3(\boldsymbol{q}^*, \boldsymbol{\alpha}, \boldsymbol{x})\big|_{x_j=\frac{A_j(\boldsymbol{q}^*)}{B_j(\boldsymbol{q}^*)},\forall j}. \end{aligned} \tag{32}$$

Again, the equality (3) holds because of the equality between $f_1(\cdots)$ and $f_3(\cdot)$ functions when x_j is chosen to appropriately. Note that $\boldsymbol{p}^*$ and $\boldsymbol{q}^*$ are feasible and optimal solutions to P1.1. Hence, the inequality (3) holds as well.

Based on (31) and (32), it is clearly evident that $f_3(\boldsymbol{q}^*, \boldsymbol{\alpha}, \boldsymbol{x})\big|_{x_j=\frac{A_j(\boldsymbol{q}^*)}{B_j(\boldsymbol{q}^*)},\forall j} = f_1(\boldsymbol{p}^*, \boldsymbol{\alpha})$ holds true. Consequently, both P1 and P1.1 have the same optimal solutions. □

APPENDIX C

Note that the P0 is decomposed into two independent resource optimization problems for NTN and TN networks. Algorithm 2 obtains transmit power allocation and UE-RBG scheduling solution for the NTN network. In what follows, we prove that such a solution is converged. The convergence of the transmit power allocation and UE-RBG scheduling for the TN network can be proved similarly. Let us denote $\{\boldsymbol{p}^{(t)}, \boldsymbol{\alpha}^{(t)}, \boldsymbol{x}^{(t)}, \boldsymbol{y}^{(t)}\}$ and $\{\boldsymbol{p}^{(t+1)}, \boldsymbol{\alpha}^{(t+1)}, \boldsymbol{x}^{(t+1)}, \boldsymbol{y}^{(t+1)}\}$ are the solutions obtained by Algorithm 2. We obtain the following set of inequalities:

$$\begin{aligned} & f_1(\boldsymbol{p}^{(t)}, \boldsymbol{\alpha}^{(t)}) \\ &\triangleq^{(a)} f_4(\boldsymbol{p}^{(t)}, \boldsymbol{\alpha}^{(t)}, \boldsymbol{x}^{(t)}, \boldsymbol{y}^{(t)}) \\ &\leq^{(b)} f_4(\boldsymbol{p}^{(t)}, \boldsymbol{\alpha}^{(t)}, \boldsymbol{x}^{(t)}, \boldsymbol{y}^{(t+1)}) \\ &\leq^{(c)} f_4(\boldsymbol{p}^{(t)}, \boldsymbol{\alpha}^{(t)}, \boldsymbol{x}^{(t+1)}, \boldsymbol{y}^{(t+1)}) \\ &\leq^{(d)} f_4(\boldsymbol{p}^{(t+1)}, \boldsymbol{\alpha}^{(t)}, \boldsymbol{x}^{(t+1)}, \boldsymbol{y}^{(t+1)}) \\ &\triangleq^{(e)} f_1(\boldsymbol{p}^{(t+1)}, \boldsymbol{\alpha}^{(t)}) \\ &\leq^{(f)} f_1(\boldsymbol{p}^{(t+1)}, \boldsymbol{\alpha}^{(t+1)}). \end{aligned} \tag{33}$$

Here, (a) is obtained by directly substituting (23) and (24) to (22); (b) is obtained using the fact that $\boldsymbol{y}^{(t+1)})$ calculated by (23) maximizes the function $f_4(\cdot)$ for the given $\boldsymbol{p}^{(t)}$, $\boldsymbol{\alpha}^{(t)}$, and $\boldsymbol{x}^{(t)}$; (b) is obtained using the fact that $\boldsymbol{x}^{(t+1)})$ calculated using (24) is the optimal solution to P1.2 for the given $\boldsymbol{p}^{(t)}$, $\boldsymbol{\alpha}^{(t)}$, and $\boldsymbol{y}^{(t+1)}$; (d) is obtained using the fact that $\boldsymbol{p}^{(t+1)})$ calculated by (26) maximizes the function $f_4(\cdot)$ for the given $\boldsymbol{\alpha}^{(t)}$, $\boldsymbol{x}^{(t+1)}$, and $\boldsymbol{y}^{(t+1)}$; (e) is obtained by applying the equality (a); (f) is obtained using the fact that $\boldsymbol{\alpha}^{(t+1)}$ determined by (29) maximizes the function $f_1(\cdot)$ for the given $\boldsymbol{p}^{(t+1)}$. The Algorithm obtains a sequence of transmit power allocation and RBG scheduling that non-decreasingly improves the network sum-rate. Since the network sum-rate is bounded above, the sequence of transmit power allocation and RBG scheduling obtained by Algorithm 2 must converge to a stable point. This completes the required proof. □

REFERENCES

[1] J.-H. Lee, J. P. Park, M. B. Bennis, and Y.-C. Ko, "Integrating LEO satellites and multi-UAV reinforcement learning for hybrid FSO/RF non-terrestrial networks," *IEEE Transactions on Vehicular Technology*, vol. 72, no. 3, pp. 3647–3662, 2023-06.

[2] N. Saeed, A. Elzanaty, H. Almorad, H. Dahrouj, T. Y. Al-Naffouri, and M.-S. Alouini, "Cubesat communications: Recent advances and future challenges," *IEEE Commun. Surveys Tuts.*, vol. 57, no. 3, pp. 14–20, 2019-05.

[3] S. Mahboob and L. Liu, "Revolutionizing future connectivity: A contemporary survey on AI-empowered satellite-based non-terrestrial networks in 6G," *ArXiv Preprint: 2303.01633*, 2022.

[4] U. Nations. [Online]. Available: https://www.un.org/techenvoy/content/global-connectivity

[5] "Solutions for NR to support non-terrestrial networks (NTN): Non-terrestrial networks (NTN) related RF and co-existence aspects," 3rd Generation Partnership Project (3GPP), Technical Report (TR), TR 38.863, March 2023, V17.2.0.

[6] "Solutions for NR to support non-terrestrial networks (NTN)," 3rd Generation Partnership Project (3GPP), Technical Report (TR), TR 38.821, May 2021, V16.1.0.

[7] "Study on New Radio (NR) to support non-terrestrial networks," 3rd Generation Partnership Project (3GPP), Technical Report (TR), TR 38.811, Sept. 2020, V15.4.0.

[8] Starlink, "Wikipedia ," 2023, accessed on June 12, 2023. [Online]. Available: https://en.wikipedia.org/wiki/Starlink

[9] Amazon, "Project Kuiper - Low Earth Orbit (LEO) mega constellation ," 2023, accessed on June 12, 2023. [Online]. Available: https://www.aboutamazon.com/what-we-do/devices-services/project-kuiper

[10] ——, "Amazon's Project Kuiper and NTT/SKY Perfect JSAT Form Strategic Collaboration to Bring Advanced Satellite Connectivity Options to Japan," *Amazon Press*, 11 2023. [Online]. Available: https://press.aboutamazon.com/2023/11/amazons-project-kuiper-and-ntt-sky-perfect-jsat-form-strategic-collaboration-to-bring-advanced-satellite-connectivity-options-to-japan

[11] Hughes, "JUPITER GEO Satellites," 2023, accessed on June 12, 2023. [Online]. Available: https://www.hughes.com/what-we-offer/satellite-services/jupiter-geo-satellites

[12] W. Abderrahim, O. Amin, M.-S. Alouini, and B. Shihada, "Proactive traffic offloading in dynamic integrated multisatellite terrestrial networks," *IEEE Transactions on Communications*, vol. 70, no. 7, pp. 4671–4686, 2022.

[13] B. Soret, I. Leyva-Mayorga, S. Cioni, and P. Popovski, "5g satellite networks for internet of things: Offloading and backhauling," *International Journal of Satellite Communications and Networking*, vol. 39, no. 4, pp. 431–444, 2021. [Online]. Available: https://onlinelibrary.wiley.com/doi/abs/10.1002/sat.1394

[14] M. Benzaghta, G. Geraci, R. Nikbakht, and D. López-Pérez, "Uav communications in integrated terrestrial and non-terrestrial networks," in *GLOBECOM 2022 - 2022 IEEE Global Communications Conference*, 2022, pp. 3706–3711.

[15] P. Cassará, A. Gotta, M. Marchese, and F. Patrone, "Orbital edge offloading on mega-leo satellite constellations for equal access to computing," *IEEE Communications Magazine*, vol. 60, no. 4, pp. 32–36, 2022.

[16] B. Shang, Y. Yi, and L. Liu, "Computing over space-air-ground integrated networks: Challenges and opportunities," *IEEE Network*, vol. 35, no. 4, pp. 302–309, 2021.

[17] J. Liu, Y. Shi, Z. M. Fadlullah, and N. Kato, "Space-air-ground integrated network: A survey," *IEEE Communications Surveys & Tutorials*, vol. 20, no. 4, pp. 2714–2741, Fourth Quarter 2018.

[18] S. Li, Q. Chen, W. Meng, and C. Li, "Civil Aircraft Assisted Space-Air-Ground Integrated Networks: An Innovative NTN of 5G and Beyond," *IEEE Wireless Communications*, vol. 29, no. 4, pp. 64–71, 2022.

[19] C. Amatetti, M. Conti, A. Guidotti, and A. Vanelli-Coralli, "NB-IoT random access procedure via NTN: system level performances," in *ICC 2022 - IEEE International Conference on Communications*, 2022, pp. 2381–2386.

[20] H.-W. Lee, A. Medles, V. Jie, D. Lin, X. Zhu, I.-K. Fu, and H.-Y. Wei, "Reverse Spectrum Allocation for Spectrum Sharing between TN and NTN," in *2021 IEEE Conference on Standards for Communications and Networking (CSCN)*, 2021, pp. 1–6.

[21] Y. Jiang, W. He, W. Liu, S. Wu, X. Wei, and Q. Mo, "A B5G Non-Terrestrial-Network (NTN) and Hybird Constellation Based Data Collection System (DCS)," *Aerospace*, vol. 10, no. 4, 2023. [Online]. Available: https://www.mdpi.com/2226-4310/10/4/366

[22] L. Liu, J. Zhang, and Z. Pi, "Inter-cell interference avoidance for downlink transmission," Aug. 7 2012, uS Patent 8,238,954.

[23] M. Rahman, Z. Hassan, J. H. Reed, and L. Liu, "Non-Terrestrial Network (NTN): a Novel Alternate Fractional Programming for the Downlink Channels Power Allocation," in *MILCOM 2023 - 2023 IEEE Military Communications Conference (MILCOM)*, 2023, pp. 963–968. [Online]. Available: https://ieeexplore.ieee.org/document/10356339

[24] K. Shen and W. Yu, "Fractional Programming for Communication Systems—Part I: Power Control and Beamforming," *IEEE Transactions on Signal Processing*, vol. 66, no. 10, pp. 2616–2630, May 2018.
[25] M. Z. Hassan, M. J. Hossain, J. Cheng, and V. C. M. Leung, "Energy-spectrum efficient content distribution in fog-ran using rate-splitting, common message decoding, and 3d-resource matching," *IEEE Transactions on Wireless Communications*, vol. 20, no. 8, pp. 4929–4946, Aug 2021.
[26] ——, "Device-clustering and rate-splitting enabled device-to-device cooperation framework in fog radio access network," *IEEE Transactions on Green Communications and Networking*, vol. 5, no. 3, pp. 1482–1501, Sept 2021.
[27] M. Z. Hassan, G. Kaddoum, and O. Akhrif, "Interference management in cellular-connected internet-of-drones network with drone clustering and uplink rate-splitting multiple access," *IEEE Internet of Things Journal*, vol. 9, no. 17, pp. 16 060–16 079, 2022.
[28] ——, "Resource allocation for joint security and interference management in noma enabled and cellular-connected internet-of-drones systems," *IEEE Transactions on Vehicular Technology*, vol. 71, no. 2, pp. 12 869–12 884, 2023.
[29] N. Mohamed, M. Z. Hassan, and G. Kaddoum, "Spectral efficiency improvement in downlink fog radio access network with deep reinforcement learning-enabled power control," *IEEE Internet of Things Journal*, vol. 10, no. 7, pp. 15 044–15 059, 2023.
[30] V. Jungnickel *et al.*, "The role of small cells, coordinated multipoint, and massive mimo in 5g," *IEEE Communications Magazine*, vol. 52, no. 5, pp. 44–51, 2014.
[31] H. Lim, J. Lee, J. Lee, S. D. Sathyanarayana, J. Kim, A. Nguyen, K. T. Kim, Y. Im, M. Chiang, D. Grunwald *et al.*, "An empirical study of 5g: Effect of edge on transport protocol and application performance," *IEEE Transactions on Mobile Computing*, vol. 23, no. 4, pp. 3172–3186, April 2023.
[32] M. Rajiullah, G. Caso, A. Brunstrom, J. Karlsson, S. Alfredsson, and O. Alay, "Carl-w: a testbed for empirical analyses of 5g and starlink performance," in *3rd ACM Workshop on 5G and Beyond Network Measurements, Modeling, and Use Cases (5G-MeMU '23)*, 2023.
[33] "Study on channel model for frequencies from 0.5 to 100 GHz," 3rd Generation Partnership Project (3GPP), Technical Report (TR), TR 38.901, December 2019, V16.1.0.
[34] Z. Yang and et al., "Optimization of rate allocation and power control for rate splitting multiple access (rsma)," *IEEE Transactions on Communications*, vol. 69, no. 9, pp. 5988–6002, September 2021.
[35] M. Z. Hassan and et al., "Joint throughput-power optimization of fog-ran using rate-splitting multiple access and reinforcement-learning based user clustering," *IEEE Transactions on Vehicular Technology*, vol. 70, no. 8, pp. 8019–8036, August 2021.
[36] A. Goldsmith, *Wireless communications*. Cambridge university press, 2005.
[37] F. C. Commission. [Online]. Available: https://spacenews.com/fcc-approves-direct-to-smartphone-regulatory-framework/
[38] "NR: User Equipment (UE) radio transmission and reception; Part 1: Range 1 Standalone (Release 18)," 3rd Generation Partnership Project (3GPP), Technical Specification (TS), TS 38.101-1, 06 2023, V18.2.0.
[39] "NR: User Equipment (UE) radio transmission and reception; Part 2: Range 2 Standalone (Release 18)," 3rd Generation Partnership Project (3GPP), Technical Specification (TS), TS 38.101-2, 06 2023, V18.2.0.
[40] "NR: Physical channels and modulation (Release 17)," 3rd Generation Partnership Project (3GPP), Technical Specification (TS), TS 38.211, 06 2023, V17.5.0.
[41] Z.-Q. Luo and S. Zhang, "Dynamic spectrum management: Complexity and duality," *IEEE Journal on Selected Topics in Signal Processing*, vol. 2, no. 1, pp. 57–73, 2008.

Md Mahfuzur Rahman (SM'18) received the B.S. degree in Electrical Engineering from Bangladesh University of Engineering and Technology (BUET), Dhaka, Bangladesh. He holds dual Master's degrees in Electrical Engineering and Physics from Michigan Technological University in Michigan. He is currently pursuing the Ph.D. Degree with The Bradley Department Of Electrical And Computer Engineering, Virginia Polytechnic, And State University, Blacksburg, VA. He has over 15 years of experience in the global wireless industry. His research interests include Non-Terrestrial Networks, Open Radio Access Networks (ORAN), and Machine Learning.

Md. Zoheb Hassan (S'15, M'23) is an Assistant Professor at the department of Electrical and Computer Engineering, Université Laval, Canada. Prior to joining Université Laval, he served as the Senior Postdoctoral Research Fellow at École de technologie Superiéure (ETS) and Research Assistant Professor within the ECE Department at Virginia Tech, USA. Dr. Hassan obtained the doctorate degree from the Electrical and Computer Engineering Department of University of British Columbia, Vancouver, Canada. He authored and co-authored over 30 journal articles and 15 conference papers in radio resource optimization, interference management, spectrum sharing, and optical wireless communications. He is the recipient NSERC Postdoctoral Fellowship Award (2021) and Four-Year Fellowship at University of British Columbia (2014). He has served/is serving as the TPC member of various prestigious IEEE Conferences, like IEEE GLOBECOM, ICC, MILCOM, VTC, and PIMRC and reviewer of several major journals of IEEE Communication Society.

Jeffrey H. Reed (Fellow, IEEE) received the B.S., M.S., and Ph.D. degrees from the University of California, Davis, CA, USA, in 1979, 1980, and 1987, respectively. He is currently the Willis G. Worcester Professor with the Bradley Department of Electrical and Computer Engineering, Virginia Tech. He is the Founder of wireless@Virginia Tech and the Founding Faculty Member of the Ted and Karyn Hume Center for National Security and Technology. He is a Fellow of the IEEE for his contributions to software radio. He is the author of three books and over 300 journal and conference papers.

Lingjia Liu (Fellow, IEEE) received the B.S. degree in electronic engineering from Shanghai Jiao Tong University and the Ph.D. degree in electrical and computer engineering from Texas A&M University. Currently, he is a Professor and the Bradley Senior Faculty Fellow with the ECE Department, Virginia Tech (VT), and also the Director of the Wireless@Virginia Tech, a center focusing on wireless technology. He spent more than four years with the Mitsubishi Electric Research Laboratory (MERL) and the Standards and Mobility Innovation Laboratory, Samsung Research America (SRA), where he received the Global Samsung Best Paper Award in 2008 and 2010. He was leading Samsung's efforts on multiuser MIMO, CoMP, and HetNets in 3GPP LTE/LTE-advanced standards. His general research interests include enabling technologies for 5G-advanced/6G networks, including incorporating domain knowledge into machine learning for wireless networks, massive MIMO, massive MTC communications, and mm-wave communications. His research received eight best paper awards. In 2021, he received the VT College of Engineering Dean's Award for Excellence in Research.